XL CILAMCE
IBERO-LATIN AMERICAN CONGRESS ON COMPUTATIONAL METHODS IN ENGINEERING
NOVEMBER 11-14, 2019
Praiamar Natal Hotel & Convention Natal, RN-BRAZIL

ASSESSMENT OF EDDY VISCOSITY MODELS IN A RESIDUAL-BASED VARIATIONAL MULTISCALE FRAMEWORK

Gabriel V. Badiola
gabrielbadiola@coc.ufrj.br
Alvaro L.G.A. Coutinho
alvaro@nacad.ufrj.br,
Renato N. Elias
rnelias@gmail.com
High Performance Computing Center and Department of Civil Engineering (NACAD)
COPPE/Federal University of Rio de Janeiro
PO Box 68506, Rio de Janeiro, RJ 21945-970, Brazil
web page: http://www.nacad.ufrj.br

Abstract. Highly turbulent flows are present in several industrial applications and natural phenomena, such as flows around aircraft airfoils and turbine blades, fluid-structure interaction problems in offshore platforms and formation of turbidity currents. In this work, a general family of eddy viscosity models (EVM) for the large-eddy simulation (LES) of turbulence is implemented in an edge-based stabilized finite element incompressible Navier-Stokes solver within the framework of the residual-based variational multiscale method (RB-VMS). We evaluate and compare the different fine-scale eddy viscosity models proposed by Oberai and Hughes. These models are incorporated into EdgeCFD, a highly optimized fully implicit parallel edge-based code, with inexact Newton solver and adaptive time step. The performance and accuracy of the proposed models are tested with validation problems for high Reynolds numbers. Results are then compared to those of highly resolved numerical simulations and experimental data and discussed.

Keywords: Turbulence, VMS, Finite Element Method, Eddy Viscosity, Computational Fluid Dynamics

1 Introduction

Fluid flows, in nature and engineering applications, are often turbulent [1,2,3]. Therefore, numerical simulation of turbulent flows is highly important for both scientific and economic reasons [1]. As examples of turbulent flows, we can mention smoke, water flowing in rivers, flows around vehicles, as well as those flows in many industrial applications like pipelines, pumps, compressors, turbines and reactors [3]. We can also mention the flows around risers, platforms, and vessels and many other fluid structure interaction problems important for the offshore industry. Despite its importance, numerical simulation of turbulent flows is still a challenge, especially for high Reynolds numbers [2].

Differently from other multiscale problems, dynamics of incompressible Newtonian flows can be described by one single set of equations for all spatial and time scales: the Navier-Stokes equations. Solving these equations numerically is a strategy called Direct Numerical Simulation (DNS). This strategy is expensive and, for many applications of interest, the computational cost remains impeditive. Studies have shown that the number of numeric operations seems to scale with the cube of Reynolds number, that means $O(Re^3)$[1].

Large-Eddy simulation (LES), on the other hand, is based on the concept of separating scales. The large scales of turbulence are solved while the effect of the small scales on the large scales is modeled. This approach offers reduced computational cost when compared to DNS, while still describing the intermittency of phenomena for the scales of interest. In that way, LES is the usual choice when DNS is unfeasible and when statistical based descriptions are not enough to represent the physical problem [1][2].

The Variational Multiscale method [4] is a general theoretical framework for computational mechanics also based on scale separation. The field to be solved is split into different scales by a direct decomposition. Inspired by LES, VMS was later applied to turbulence [5]. The variable of interest is split into resolved scales and one unresolved subscale. The subscale can be determinate, among other strategies, by methods based on projection (OSS - Orthogonal subgrid scale) and on the residual of the resolved scales (RB-VMS) [6]. Like OSS, the Residual-Based Variational Multiscale Method (RB-VMS) presents the advantage of being consistent. Since the effect of the unresolved scales is modeled based on the residual of the large scales, once the resolved scales are able to fully represent the field, the contribution of the subscale vanishes. Another advantage of this method is its analogies with standard stabilized methods for advection-dominated flows, like Streamline-Upwind Petrov–Galerkin/Pressure stabilizing Petrov–Galerkin/Least-Squares Incompressibility Constraint (SUPG/PSPG/LSIC). This analogy allows straightforward extensions of existing computer codes [2][6].

A mathematical closure problem arises from every method relying on scale separation e.g. LES, VMS and RANS (Reynolds-Averaged Numerical Simulation) [1]. One usual way to solve this closure problem, especially for methods based on one resolved scale and one unresolved scale, is defining a subgrid scale viscosity. These viscosity models, also called, eddy viscosity models (SGS) are widely used, the most popular being the Smagorinsky model. The eddy viscosity model proposed by Smagorinsky is proportional to the magnitude of the strain tensor local rate calculated with the resolved scales. That means that, adding this viscosity to the equations of the resolved scales, adds inconsistencies to the method.

It was observed [8][9] that RB-VMS formulation under predicts the contribution of the subgrid scale on the resolved scale. To address this issue, Oberai and Liu [8][9] proposed adding eddy-viscosity model to the RB-VMS formulation. This strategy was tested for compressible and incompressible flows using a spectral framework and applying an eddy viscosity model calculated with the subgrid velocity. The fact that the viscosity model depends on the subgrid velocity has the advantage of keeping consistency and being inherently dynamic. The results obtained with this viscosity and RB-VMS are better results than RB-VMS by itself.

Hughes and Oberai [10] present a family of eddy viscosity models for VMS intended to be applied only in the fine resolved scales, when splitting the field in more than one resolved scale. Requiring Galilean invariance and dimensional consistency, they came up with a general expression for eddy viscosities inspired by the Smagorinsky model.

In this study we propose using RB-VMS framework with two scales: one large resolved scale and one fine unresolved subgrid scale. In addition to that we apply some of the eddy viscosity models proposed by Hughes and Oberai [10], considering as the fine scale our unresolved scale. Different eddy viscosity models are tested and the results are compared with those obtained with SUPG/PSPG/LISC with Smagorinsky eddy viscosity and those obtained with RB-VMS with no eddy viscosity. The paper is organized as follows: the applied methods are presented in Section 2, some comments about the implementation are made in the Section 3, the results are presented in Section 4 and, finally, conclusions and discussions are presented in Section 5.

2 Methods

2.1 Governing equations

Considering a spatial domain $\Omega \subset \mathbb{R}^3$ with a piecewise regular boundary Γ and a time interval $[0, t_f]$, the Navier-Stokes equations governing the flow of incompressible viscous fluids are given by:

$$\rho\left(\frac{\partial \boldsymbol{u}}{\partial t} + \boldsymbol{u}\cdot\nabla\boldsymbol{u}\right) - \boldsymbol{f} - \nabla\cdot\boldsymbol{\sigma} = \boldsymbol{0} \qquad on\ \Omega\times[0,t_f], \tag{1}$$

$$\nabla\cdot\boldsymbol{u} = \boldsymbol{0} \qquad on\ \Omega\times[0,t_f], \tag{2}$$

where $\boldsymbol{u}$ is the velocity field, ρ is the fluid density, $\boldsymbol{\sigma}$ is the stress tensor and $\boldsymbol{f}$ is the external forces vector.

Equation (1) can be rewritten as:

$$\rho\left(\frac{\partial \boldsymbol{u}}{\partial t} + \boldsymbol{u}\cdot\nabla\boldsymbol{u}\right) - \boldsymbol{f} + \nabla p - \rho\nu\nabla^2\boldsymbol{u} = \boldsymbol{0} \quad on\ \Omega\times[0,t_f]. \tag{3}$$

The stress tensor is defined as:

$$\boldsymbol{\sigma}(p,\boldsymbol{u}) = -p\boldsymbol{I} + \boldsymbol{T}, \tag{4}$$

where $\boldsymbol{I}$ is the identity tensor and $\boldsymbol{T}$ is the deviatoric stress tensor, stated as:

$$\mathbf{T} = 2\mu\boldsymbol{\varepsilon}(\boldsymbol{u}) = 2\rho\nu\boldsymbol{\varepsilon}(\boldsymbol{u}). \tag{5}$$

In this equation, μ is the dynamic viscosity, ν is the kinematic viscosity and $\boldsymbol{\varepsilon}(\boldsymbol{u})$ is the strain rate tensor defined as follows:

$$\boldsymbol{\varepsilon}(\boldsymbol{u}) = \frac{1}{2}(\nabla\boldsymbol{u} + (\nabla\boldsymbol{u})^T). \tag{6}$$

In our case the kinematic viscosity ν is composed of two parts:

$$\nu = \nu_{phys} + \nu_T, \tag{7}$$

where ν_{phys} represents the physical kinematic viscosity, physical property of the fluid, and ν_T is the added eddy viscosity calculated using the models described in the following sections.

The Dirichlet (essential) and Neumann (natural) boundary conditions associated with the problem are applied on the complementary subsets Γ_g and Γ_h of the boundary $\Gamma = \Gamma_g \cup \Gamma_h$, $\Gamma_g \cap \Gamma_h = \emptyset$ and are given by:

$$\boldsymbol{u} = \boldsymbol{g} \qquad on\ \Gamma_g, \tag{8}$$

$$\boldsymbol{n} \cdot \boldsymbol{\sigma} = \boldsymbol{h} \qquad on\ \Gamma_h, \tag{9}$$

where $\boldsymbol{g}$ and $\boldsymbol{h}$ are given functions and $\boldsymbol{n}$ is the unit outward normal vector of the boundary Γ.

The initial condition is defined as:

$$\boldsymbol{u}(\boldsymbol{x}, 0) = \boldsymbol{u_0} \qquad \boldsymbol{x} \in \Omega_0. \tag{10}$$

2.2 Variational multiscale method

In a two-scale variational multiscale method (VMS) for large eddy simulation (LES) the flow fields are decomposed into coarse (resolved) and fine (unresolved) scales:

$$\boldsymbol{u} = \boldsymbol{u}^h + \boldsymbol{u}', \tag{11}$$

$$p = p^h + p', \tag{12}$$

where $(\boldsymbol{u^h}, p^h)$ and $(\boldsymbol{u}', p')$ stand for the coarse and fine scale components of the solution, respectively.

This can be seen as a direct sum decomposition of infinite-dimension spaces:

$$U^* = U^h \oplus U', \tag{13}$$

$$P^* = P^h \oplus P', \tag{14}$$

$$V^* = U^* \times P^* = V^h \oplus V', \tag{15}$$

where

$$(\boldsymbol{u}, p) \in V^* = U^* \times P^*. \tag{16}$$

The coarse scale, in this work, is directly associated with the finite element approximation obtained by the discretization of the spatial domain.

In the case of RB-VMS, the fine scales are given by:

$$\boldsymbol{u}' = -\tau_M \boldsymbol{r_M}, \tag{17}$$

$$p' = -\tau_C r_C, \tag{18}$$

where $\boldsymbol{r_M}$ is the residual of the Navier-Stokes momentum equation and $\boldsymbol{r_C}$is the residual of the Navier-Stokes continuity equation. τ_M and τ_C are algebraic parameters to be set. These parameters can be related to the ones in stabilized finite element formulations. In this work we define:

$$\tau_M = \left(\frac{4}{\Delta t^2} + \left(\frac{\|\boldsymbol{u}^h\|}{h} \right)^2 + 9 \left(\frac{\nu}{h^2} \right)^2 \right)^{-1/2}, \tag{19}$$

$$\tau_C = \frac{h}{3} \|\boldsymbol{u}^h\|. \tag{20}$$

Here h is a length scale related to the element size. In this work, we consider:

$$h = (Vol_{el})^{1/3}, \tag{21}$$

where Vol_{el} is the volume of a finite element.

The residual $\boldsymbol{r_M}$ and $\boldsymbol{r_C}$ are obtained from Eq. (3) and Eq. (2) and can be stated as:

$$\boldsymbol{r_M} = \rho \left(\frac{\partial \boldsymbol{u^h}}{\partial t} + \boldsymbol{u}^h \cdot \nabla \boldsymbol{u}^h \right) - \boldsymbol{f} + \nabla p - \rho \nu \boldsymbol{\nabla^2 u}^h, \tag{22}$$

$$r_C = \boldsymbol{\nabla \cdot u^h}. \tag{23}$$

2.3 Finite element formulation

The weak form of the Navier-Stokes equations can be stated as:

Find $(\boldsymbol{u}, p) \in V^* = U^* \times P^*, \forall (\boldsymbol{w}, q) \in Z^* = W^* \times Q^*$ such that we have:

$$\begin{aligned} \int_\Omega \boldsymbol{w} \cdot \left[\rho \left(\frac{\partial \boldsymbol{u}}{\partial t} + \boldsymbol{u} \cdot \nabla \boldsymbol{u} \right) - \boldsymbol{f} \right] d\Omega + \int_\Omega \boldsymbol{\varepsilon}(\boldsymbol{w}) : \boldsymbol{\sigma}(p, \boldsymbol{u}) d\Omega \\ + \int_\Omega q \, \boldsymbol{\nabla \cdot u} \, d\Omega - \int_{\Gamma_h} \boldsymbol{w} \cdot \boldsymbol{h} \, d\Gamma = 0, \end{aligned} \tag{24}$$

where:

$$U^* = \{ \boldsymbol{u}(\boldsymbol{x}, t) | \boldsymbol{u}(\boldsymbol{x}, t) \in H^1(\Omega)^3; \boldsymbol{u} = \boldsymbol{g} \; on \; \Gamma_g \}, \tag{25}$$

$$P^* = \left\{ p(\boldsymbol{x}, t) | p(\boldsymbol{x}, t) \in L^2(\Omega); \int_\Omega p \, d\Omega = 0 \; if \; \Gamma = \Gamma_g \right\}, \tag{26}$$

$$W^* = W^h \oplus W' = \{ \boldsymbol{w}(\boldsymbol{x}, t) | \boldsymbol{w}(\boldsymbol{x}, t) \in H^1(\Omega)^3; \boldsymbol{w} = \boldsymbol{0} \; on \; \Gamma_g \}, \tag{27}$$

$$Q^* = Q^h \oplus Q' = P^*. \tag{28}$$

$U^h \subset U^*$, $P^h \subset P^*$, $W^h \subset W^*$ and $Q^h \subset Q^*$ are finite dimension spaces associated with the finite element approximation of the problem.

Replacing $\boldsymbol{u}$ and p by their VMS decomposition defined by Eq. (11) and Eq. (12) and $\boldsymbol{w}$ by $\boldsymbol{w} = \boldsymbol{w}^h + \boldsymbol{w}'$, we obtain:

$$\begin{aligned}\int_\Omega \boldsymbol{w}^h \cdot \left[\rho\left(\frac{\partial(\boldsymbol{u}^h+\boldsymbol{u}')}{\partial t} + (\boldsymbol{u}^h+\boldsymbol{u}')\cdot\nabla(\boldsymbol{u}^h+\boldsymbol{u}')\right) - \boldsymbol{f}\right] d\Omega \\ + \int_\Omega \boldsymbol{\varepsilon}(\boldsymbol{w}^h) : \boldsymbol{\sigma}(p+p', \boldsymbol{u}^h+\boldsymbol{u}') d\Omega \\ + \int_\Omega q^h\, \boldsymbol{\nabla}\cdot(\boldsymbol{u}^h+\boldsymbol{u}')\, d\Omega - \int_{\Gamma_h} \boldsymbol{w}^h\cdot\boldsymbol{h}\, d\Gamma = 0.\end{aligned} \tag{29}$$

Considering that linear finite elements are used to represent the large scales and that the functions representing the fine scales vanish on element boundaries, after some manipulation, we obtain:

$$\begin{aligned}\int_\Omega \boldsymbol{w}^h \cdot \rho\frac{\partial \boldsymbol{u}^h}{\partial t}\, d\Omega + \int_\Omega \boldsymbol{w}^h \cdot \left[\rho(\boldsymbol{u}^h - \tau_M \boldsymbol{r_M})\cdot\boldsymbol{\nabla}\boldsymbol{u}^h\right] d\Omega \\ + \int_\Omega \boldsymbol{\varepsilon}(\boldsymbol{w}^h) : \boldsymbol{\sigma}(p^h, \boldsymbol{u}^h) d\Omega + \int_\Omega q^h\, \boldsymbol{\nabla}\cdot\boldsymbol{u}^h\, d\Omega \\ + \int_\Omega \frac{1}{\rho}\tau_M \boldsymbol{r_M} \cdot \left[\rho(\boldsymbol{u}^h - \tau_M \boldsymbol{r_M})\cdot\boldsymbol{\nabla}\boldsymbol{u}^h + \nabla q^h\right] d\Omega \\ + \int_\Omega \tau_C\,(\boldsymbol{\nabla}\cdot\boldsymbol{u}^h)\rho(\boldsymbol{\nabla}\cdot\boldsymbol{w}^h) - \int_{\Gamma_h} \boldsymbol{w}^h\cdot\boldsymbol{h}\, d\Gamma - \int_\Omega \boldsymbol{f} d\Omega = 0.\end{aligned} \tag{30}$$

We can define:

$$\boldsymbol{u}^* = \boldsymbol{u}^h + \boldsymbol{u}' = \boldsymbol{u}^h - \tau_M \boldsymbol{r_M}. \tag{31}$$

Replacing (31) in (30),

$$\begin{aligned}\int_\Omega \boldsymbol{w}^h \cdot \rho\frac{\partial \boldsymbol{u}^h}{\partial t}\, d\Omega + \int_\Omega \boldsymbol{w}^h \cdot (\rho\boldsymbol{u}^*\cdot\boldsymbol{\nabla}\boldsymbol{u}^h)\, d\Omega + \int_\Omega \boldsymbol{\varepsilon}(\boldsymbol{w}^h) : \boldsymbol{\sigma}(p^h, \boldsymbol{u}^h) d\Omega \\ + \int_\Omega q^h\, \boldsymbol{\nabla}\cdot\boldsymbol{u}^h\, d\Omega \\ + \int_\Omega \frac{1}{\rho}\tau_M \boldsymbol{r_M} \cdot (\rho\boldsymbol{u}^*\cdot\boldsymbol{\nabla}\boldsymbol{u}^h + \nabla q^h)\, d\Omega \\ + \int_\Omega \tau_C\,(\boldsymbol{\nabla}\cdot\boldsymbol{u}^h)\rho(\boldsymbol{\nabla}\cdot\boldsymbol{w}^h) - \int_{\Gamma_h} \boldsymbol{w}^h\cdot\boldsymbol{h}\, d\Gamma \\ - \int_\Omega \boldsymbol{f} d\Omega = 0.\end{aligned} \tag{32}$$

2.4 SUPG/PSPG/LSIC

The SUPG/PSPG/LSIC formulation for the Navier-Stokes equations, considering linear elements and $\tau_{SUPG} = \tau_{PSPG} = \tau_{SUPG/PSPG}$ is given by:

$$\begin{aligned}\int_{\Omega} \boldsymbol{w}^h \cdot \rho \frac{\partial \boldsymbol{u}^h}{\partial t}\, d\Omega + \int_{\Omega} \boldsymbol{w}^h \cdot \left(\rho \boldsymbol{u}^h \cdot \boldsymbol{\nabla} \boldsymbol{u}^h\right) d\Omega + \int_{\Omega} \boldsymbol{\varepsilon}(\boldsymbol{w}^h) : \boldsymbol{\sigma}(p^h, \boldsymbol{u}^h) d\Omega \\ + \int_{\Omega} q^h\, \boldsymbol{\nabla} \cdot \boldsymbol{u}^h\, d\Omega \\ + \int_{\Omega} \frac{1}{\rho} \tau_{SUPG/PSPG} \boldsymbol{r_M} \cdot \left(\rho \boldsymbol{u}^h \cdot \boldsymbol{\nabla} \boldsymbol{u}^h + \nabla q^h\right) d\Omega \\ + \int_{\Omega} \tau_{LSIC} \left(\boldsymbol{\nabla} \cdot \boldsymbol{u}^h\right) \rho \left(\boldsymbol{\nabla} \cdot \boldsymbol{w}^h\right) d\Omega - \int_{\Gamma_h} \boldsymbol{w}^h \cdot \boldsymbol{h}\, d\Gamma \\ - \int_{\Omega} \boldsymbol{f} d\Omega = 0.\end{aligned} \tag{33}$$

Equation (32) is quite similar to Eq. (31), except for the modified advection velocity $\boldsymbol{u}^*$ and the stabilization parameters. As discussed in details in [2], this analogy allows RB-VMS to be implemented straightforward from SUPG/PSPG/LSIC implementations for linear elements.

2.5 Eddy viscosity models

A family of eddy viscosity models for VMS was proposed by Oberai and Hughes [10]. This family was initially intended to be applied only in the fine resolved scales, when the solution fields are split in multiple scales.

The multilevel approach, consisting of splitting the resolved scales in large resolved scales and fine resolved scales is especially suited for spectral methods. For other discrete approximation, e.g. finite element method, a fine-scale projection operator needs to be implemented. This requires complex algorithms to be implemented, like geometric and algebraic multigrid solvers [10].

In this work, we apply a two-scale RB-VMS framework: one resolved scale and one unresolved scale. When using the proposed eddy viscosity models, we consider our unresolved scale as the fine scale. The main idea is to test Smagorinsky-like eddy viscosity models based on both the resolved and the unresolved scales. Since in the RB-VMS framework the unresolved scales are modeled by the residual of the resolved scales, the viscosities models based on the unresolved scales vanish when the resolved scales are accurate enough. This preserves the method's consistency. The viscosity is applied in all the resolved scales.

In the most general case, eddy viscosities can be written as:

$$\nu_T = C^2 h^n \left|\nabla^S \boldsymbol{u}^h\right|^p |\nabla^S \boldsymbol{u}'|^q |\boldsymbol{u}'|^r \left|\boldsymbol{u}^h\right|^m, \tag{34}$$

where C is a non-dimensional parameter, h is a length scale, ∇^S is the symmetric gradient operator and m, n, p, q and r are exponents to defined.

Requiring Galilean invariance, we obtain:

$$\nu_T = C^2 h^n \left|\nabla^S \boldsymbol{u}^h\right|^p |\nabla^S \boldsymbol{u}'|^q |\boldsymbol{u}'|^r . \tag{35}$$

Requiring dimensional consistency, we obtain:

$$\nu_T = C^2 h^{2-r} \left|\nabla^S \boldsymbol{u}^h\right|^p |\nabla^S \boldsymbol{u}'|^{1-p-r} |\boldsymbol{u}'|^r. \tag{36}$$

From Eq. (34), we can state that the turbulent viscosity is defined by a two-parameter (p, r) family of functions. A schematic representation of the two-parameter space of models is presented in Fig. 1. The triangle with vertices (0, 0), (1, 0), and (1, 1) contain the models we are most interested in testing.

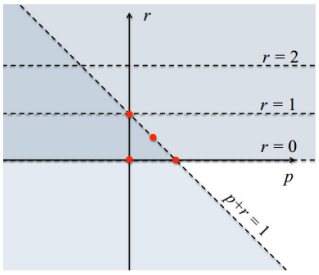

Figure 1- two-parameter space of models [10]

The value of C is not arbitrary and can be calculated by computing the model dissipation. For the Smagorinsky, this value was calculated by Lilly [14] and lies in the ranges 0.1 – 0.2 [11]. In [7] C equals 0.15 is used for an eddy viscosity based on the norm of the small scale. The same is done in [8]. Briefly, values between 0.1 and 0.2 can be considered to be a reasonable choice for this parameter. In this paper, we use C equals 0.1 for all tested models. h is a length scale related to the element size. In this work, we consider it as the cubic root of a finite element volume, as stated in Eq. (19).

Is it worth mentioning that, since C is considered to be a positive number, these models only take into account energy transferred from the resolved scales to the unresolved scales. Although this is true in many cases, the transfer of energy in the opposite way exists (backscattering) and can be important for specific problems.

2.6 Specific eddy viscosity models

EVM-RB-VMS-1 Turbulent energy-like model

Choosing $r = 1$ and $p = 0$ yields the following model:

$$\nu_T = C^2 h |\boldsymbol{u}'|, \tag{37}$$

where $\boldsymbol{u}'$, defined by Eq. (17), depends on the residual of the resolved scales.

As previously mentioned, the fact that the model depends on the magnitude of the unresolved scale assure consistency to the resulting RB-VMS formulation with eddy viscosity (EVM-RB-VMS). This model was tested in [7] and in [8], where it was called residual-based eddy viscosity RB-EVM. Due to its relation to turbulent energy, we decide to call it “turbulent energy”-like model.

EVM-RB-VMS-2 Small-large

Choosing $r = 0$ and $p = 0$ yields the following model:

$$\nu_T = C^2 h^2 |\nabla^S \boldsymbol{u}'|. \tag{38}$$

EVM-RB-VMS-3 Large-large

Choosing $r = 0$ and $p = 1$ yields the following model:

$$\nu_T = C^2 h^2 \left|\nabla^S \boldsymbol{u}^h\right|, \tag{39}$$

that is the Smagorinsky eddy viscosity model. It is worth mentioning that this model introduces inconsistencies to the resulting EVM-RB-VMS formulation.

EVM-RB-VMS-4 Plateau

Choosing $r = 1/2$ and $p = 1/2$ yields the following model:

$$\nu_T = C^2 h^{3/2} \left|\nabla^S \boldsymbol{u}^h\right|^{1/2} |\boldsymbol{u}'|^{1/2}. \tag{40}$$

Due to its dependence on $|\boldsymbol{u}'|^{1/2}$, this model can be seen as a Smagorinsky-like model that modulates the decay rate of the eddy viscosity (a plateau in the wavenumber space) [10].

EVM-RB-VMS-5 DCDD-like

Choosing $r = 2$ and $p = 1$ yields the following model:

$$\nu_T = C^2 \left|\nabla^S \boldsymbol{u}^h\right| |\nabla^S \boldsymbol{u}'|^{-2} |\boldsymbol{u}'|^2. \tag{41}$$

This model resembles the discontinuity-capturing directional dissipation (DCDD) viscosity described in [18]. This model presents potential instability because $|\nabla^S \boldsymbol{u}'|$ appears in the denominator. Regularization by adding a small positive constant to the denominator was applied to avoid this problem.

EVM-RB-VMS-6 One-one

Choosing $r = 1$ and $p = 1$ yields the following model:

$$\nu_T = C^2 h \left|\nabla^S \boldsymbol{u}^h\right| |\nabla^S \boldsymbol{u}'|^{-1} |\boldsymbol{u}'|. \tag{42}$$

This model presents potential instability and regularization is also applied.

3 Implementation

The formulation presented in this work was implemented in EdgeCFD, an in-house software developed at the High-Performance Computer Center (NACAD) at COPPE/UFRJ. EdgeCFD is a parallel optimized code written in Fortran90, consisting of edge-based implementation of stabilized finite element method and RB-VMS for incompressible and compressible flows and transport equation. The stabilized finite element formulation applied is SUPG/PSPG/LSIC, which is also adapted to RB-VMS [2]. When SUPG/PSPG/LSIC is used, turbulence is modeled by classic Smagorinsky (LES).

Inexact-Newton Krylov Method is used for the non-linear solver and generalized minimal residual method (GMRES) is used for the linear solver. Time step adaptivity is implemented using a PID controller. Nodal-block diagonal preconditioner is employed for the flow equations. When transport equations are solved, diagonal preconditioner is employed for the transport equations. Integrals are computed using closed form relations derived in volume coordinates or using a one-point integration rule. That means all coefficients in the element matrices and residuals are explicitly coded. Distributed and shared parallelism paradigms (MPI and OpenMP) are considered throughout the whole code.

EdgeCFD and its extensions also allow simulation of free surface flows using Volume-of-Fluid (VOF) or level sets, Non-Newtonian flows using Power Law, Bingham and Hershel-Buckley and Fluid-Structure Interaction and Multiphase flows. More recently, mesh refinement through mesh multiplication was incorporated [15][16].

4 Results

4.1 Flow around a circular cylinder

The previously presented formulations are applied to the solution of the turbulent flow around a circular cylinder with Reynolds number (Re) equals to 1000. In this classical problem, the flow past a circular cylinder causes vortex shedding.

For this problem, the Reynolds number can be defined as:

$$Re = \rho UD/\mu = UD/\nu. \tag{43}$$

Here ρ is the fluid density, U is magnitude of the inflow velocity, D is the cylinder diameter, μ is the fluid dynamic viscosity and ν is the fluid kinematic viscosity.

The Reynolds number can be seen as a ratio of inertial and viscous effects. The greater the Reynolds number is, more turbulent is the flow.

Another dimensionless number important to describe the flow around a cylinder with vortex shedding is the Strouhal number, defined as:

$$St = f_s D/U, \tag{44}$$

where f_s is the frequency of vortex shedding, D is the cylinder diameter and U is the inflow velocity.

The relationship between Reynolds number and Strouhal number is known from experiments for circular cylinders in two-dimensions flow conditions, as shown in Fig. 2. We can note that Strouhal is close to 0.2 for a large range of Reynolds number, including the one we are testing here. It is also known that Strouhal number depends also on other aspects like the cylinder rugosity and cylinder aspect ratio, which is the ratio between cylinder diameter and length.

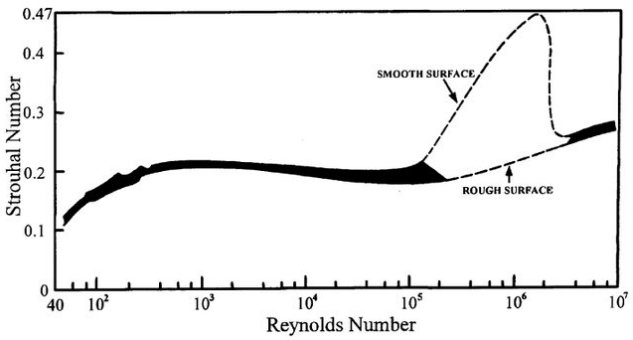

Figure 2 - relationship between Reynolds and Strouhal [19]

Vortex shedding is also closely related to lift and drag forces on the cylinder, defined as:

$$\boldsymbol{t} = \int_{\Gamma_{cyl}} \boldsymbol{n} \cdot \boldsymbol{\sigma}\, d\Gamma, \tag{45}$$

$$F_L = \boldsymbol{t} - \boldsymbol{t} \cdot \left(\frac{\boldsymbol{U}}{U}\right), \tag{46}$$

$$F_D = \boldsymbol{t} \cdot \left(\frac{\boldsymbol{U}}{U}\right), \tag{47}$$

where $\boldsymbol{t}$ is the tension vector acting on the cylinder lateral surface, Γ_{cyl} is the cylinder surface, $\boldsymbol{n}$ is the unit outward normal, $\boldsymbol{U}$ is the inflow velocity vector and U is its magnitude. Also $\boldsymbol{\sigma}$ is the stress tensor and is defined in Eq. (4).

Lift and drag coefficients are dimensionless numbers, given by:

$$C_L = \frac{2F_L}{\rho L D U^2}, \tag{48}$$

$$C_D = \frac{2F_D}{\rho L D U^2}, \tag{49}$$

where ρ is the fluid density, L is the cylinder length, D is the cylinder diameter, F_L is the lift force and F_D is the drag force.

In the case of the flow around a circular cylinder, even though there is periodic shedding from alternating sides of the body, due to symmetry, the time-averaged lift coefficient is zero. Because of that, usually, we are interested in fluctuating lift coefficient [24], defined as:

$$C'_{L_{rms}} = \frac{2F'_L}{\rho L D U^2}, \tag{50}$$

where F'_L is the root-mean-square lift force fluctuations.

The time-averaged drag coefficient, on the other hand, is not zero. Because of that, usually, we are interested in the mean drag coefficient, defined as:

$$\overline{C_D} = \frac{2\overline{F_D}}{\rho L D U^2}, \tag{51}$$

where $\overline{F_D}$ is time-averaged drag force.

Relationships between Reynolds number and fluctuating lift coefficient for a smooth cylinder, obtained experimentally and numerically, are shown in Fig. 3. From experiments, fluctuating lift coefficient would be approximately 0.05 for Reynolds number equals 1000. Nevertheless, results obtained numerically doesn't seem to match that, lying in a wide range of values between 0.1 and 0.7.

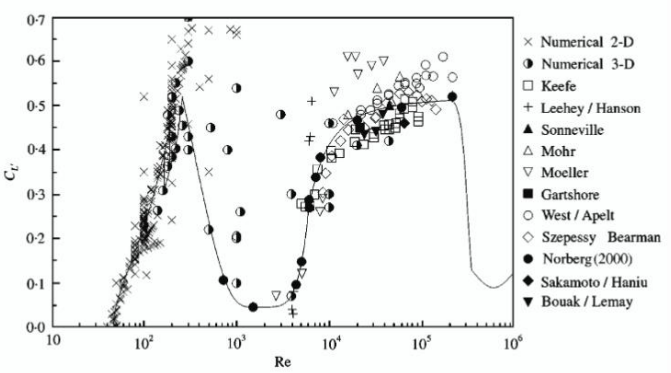

Figure 3 - relationship between Reynolds and root-mean-square fluctuating lift coefficient [24][25]

The relationship between Reynolds number and drag coefficient is known for smooth circular cylinders in two-dimensions flow conditions, as shown in Fig. 4. We can note that for Reynolds number equals 1000, drag coefficient is close to 1.0. Like the Strouhal number, the drag coefficient also depends on other aspects like the cylinder rugosity.

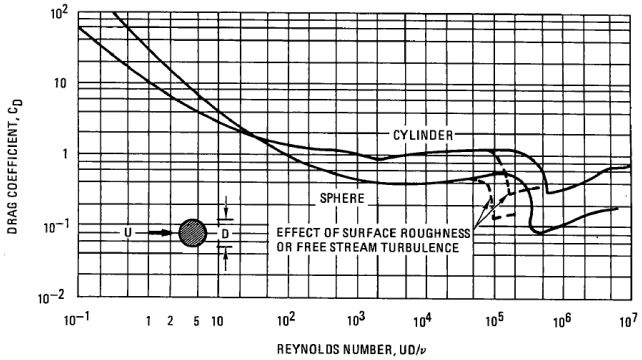

Figure 4 – relationship between Reynolds and drag coefficient [19][23]

In this work Re, St, $\overline{C_D}$ and $C'_{L_{rms}}$ are used to evaluate the results obtained when employing the different formulations presented.

4.2 Test case

As presented in the previous section, the physical problem we use as test case consists of the well-known incompressible flow around a smooth circular cylinder, in our case, with Reynolds number equals to 1000. According to the physics of the problem, the domain would be infinity in both x and y directions. Considering that the domain is also infinity in the z direction implies that the velocity should be invariant in this direction, what would allow using bidimensional domains to represent the geometry of the problem. Although, when dealing with turbulence, it is more usual to use tridimensional domains.

In this paper we choose to represent the geometry as a tridimensional domain. To reduce computational time, the domain has to be truncated. The dimensions of the geometry used for the numerical model is presented in Fig. 5. The length is 28 times the cylinder diameter ($28D$), the width is 16 times the cylinder diameter ($16D$) and the height, which is equal to the cylinder length, is 8 times the cylinder diameter ($8D$). The distance between the cylinder centerline and the inflow boundary is 8 times the diameter ($8D$). A fluid with density ρ and dynamic viscosity ν flows past a circular cylinder with diameter D and length $L = 8D$ with inflow velocity with magnitude U. The boundary conditions are: prescribed velocity in the inflow boundary, null pressure is prescribed in the outflow boundary (null tension condition), no slip conditions in the walls of the cylinder and no penetrability condition in the parallel lateral boundaries of the domain, as shown in Fig. 6. As initial condition, we consider null velocity for the whole domain. In our case, we also consider: $\rho = 1, \nu = 1.0 \times 10^{-3}, \mu = 1.0 \times 10^{-3}$, $D = 1, L = 8$ and $U = 1$, resulting in $Re = \rho UD/\mu = UD/\nu = 1000$.

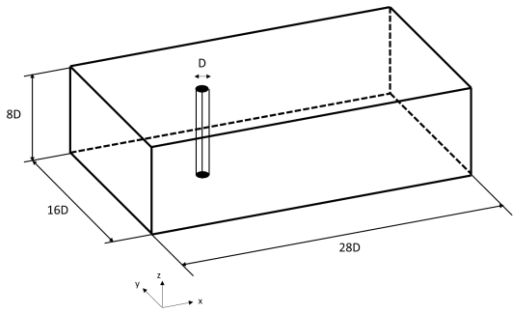

Figure 5 – tridimensional domain

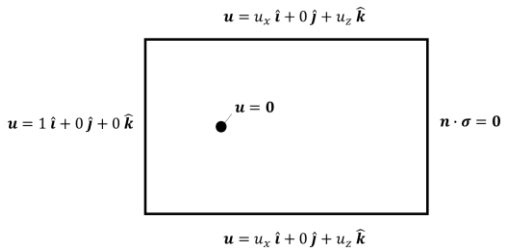

Figure 6 – applied boundary conditions

The used mesh consists of 1,862,078 elements and 320,562 nodes and is presented in Fig. 6. and Fig. 7. The simulations were run in Lobo Carneiro super computer using 12 processors. The resulting mesh partitions for one simulation is presented in Fig. 8.

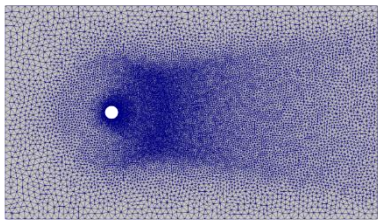

Figure 6 – full mesh

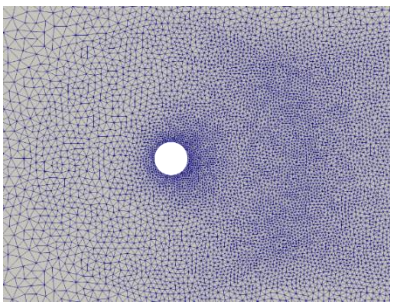

Figure 7 – mesh around the cylinder

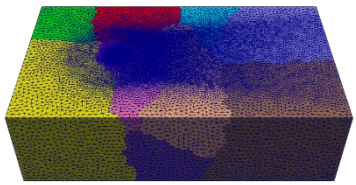

Figure 8-mesh partitions

As numerical solution parameters we use: constant time step of 0.025 with a total number of steps equal to 80,000; the nonlinear loops are stopped after a decrease of four orders of magnitude of the relative and absolute residua. The number of Krylov vectors for the nodal block-diagonal preconditioned GMRES solver is 35. It is worth mentioning that the 0.025 fixed time-step was estimated after an initial Reynolds ramping step run with PID adaptative time step. During this step, the inflow velocity is slowly increased until the final Reynolds number is achieved.

4.3 Results

Results and computational times are presented in Table 1. For each formulation, time-averaged drag coefficient, time-averaged lift coefficient, root-mean-square lift force fluctuations and Strouhal number are presented, as well as the total wall time of both the Reynolds ramp step and the 80.000 iterations with fixed time increment. In Fig.9 and Fig.10, lift and drag coefficients are plotted over time for each of the formulations.

Table 1. Results and computational times

Formulation	$\overline{C_D}$	$\overline{C_L}$	$C'_{L_{rms}}$	St	wall time (DD:HH:MM:SS)
SUPG/PSPG/LSIC +Smagorinsky	1.2291	0.0094894	0.37641	0.19997	00:16:091:09
RB-VMS	1.2278	0.0001406	0.38323	0.19997	00:18:53:17
EVM-RB-VMS-1 Turbulent energy-like	1.2149	0.0077212	0.34385	0.19485	00:10:22:32
EVM-RB-VMS-2 Small-large	1.2328	0.0039698	0.37372	0.19997	00:23:25:33
EVM-RB-VMS-3 Large-large	1,2295	0.0089938	0.34532	0.19485	01:06:44:47
EVM-RB-VMS-4 Plateau	1.1886	0.0113560	0.28525	0.19485	01:08:37:59
EVM-RB-VMS-5 DCDD-like	1.2105	0.0066287	0.31335	0.19485	00:18:26:11
EVM-RB-VMS-6 One-one	-	-	-	-	-
Numerical Reference [21]	1.41	-	-	0.23	-
Numerical Reference [25]	-	-	0.1 - 0.7	-	-
Experimental [20]	1.48	-	-	0.25	-
Experimental [19][25] (Fig. 2, Fig. 3 and Fig. 4)	1.0	-	0.05	0.2	-

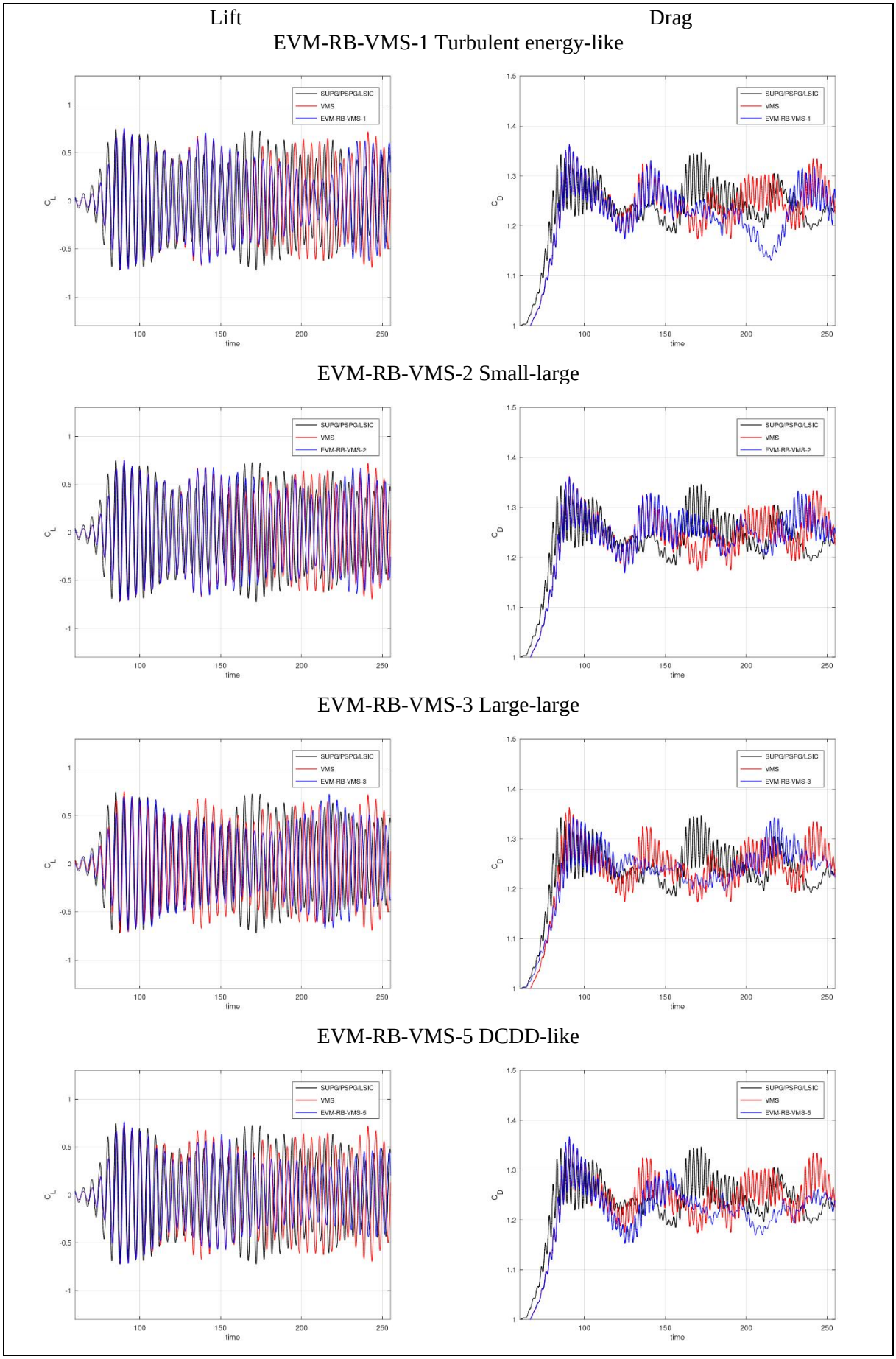

Figure 9-Lift and Drag coefficients

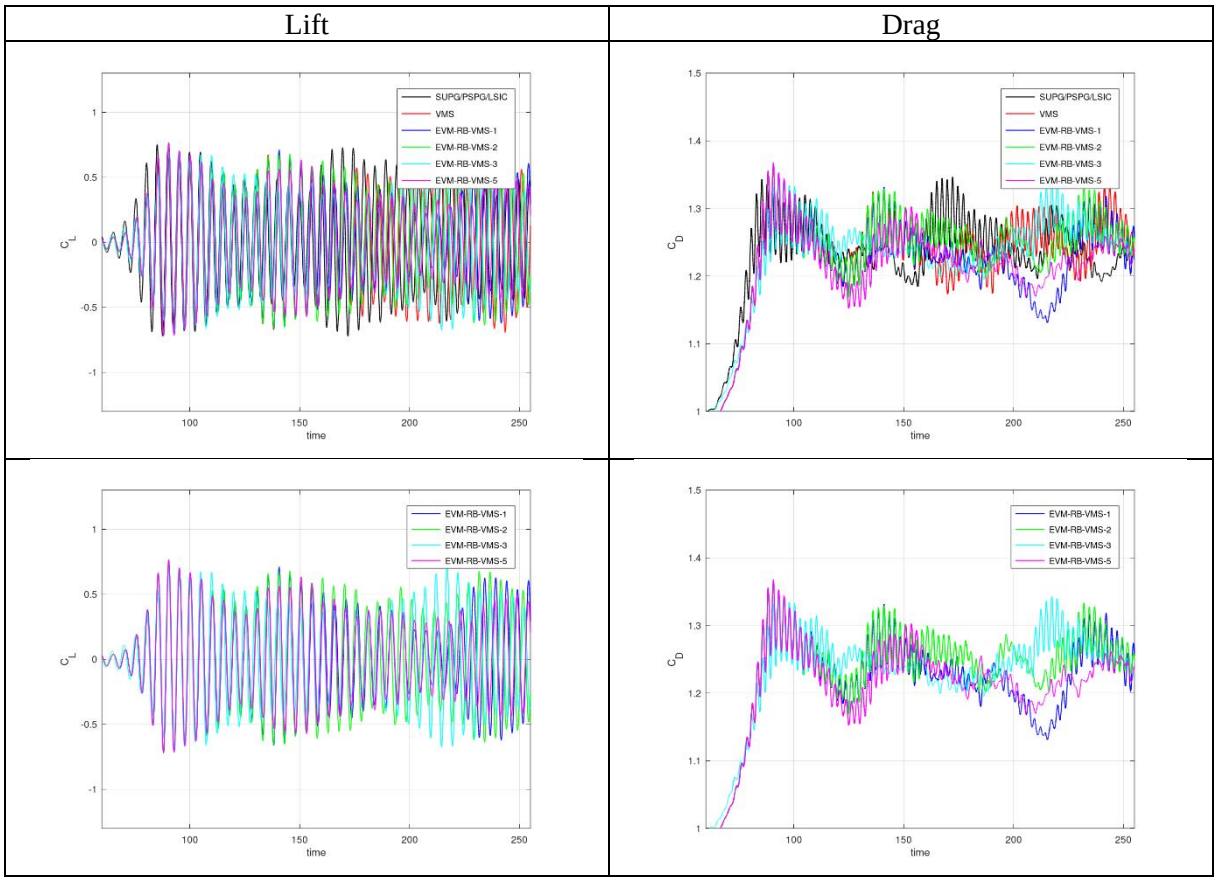

Figure 10-Lift and Drag coefficients

From Table 1, Fig. 9 and Fig. 10, we can see that the presented formulations (EVM-RB-VMS) were able to represent the flow around the cylinder at least as well as the already implemented SUPG/PSPG/LSIC with Smagorinsky and RB-VMS formulations. From Fig. 2, we can see that for Reynolds 1000, from experiments, $St \sim 0.2$. From Fig. 3, we can see that $\overline{C_D} \sim 1$ and from Fig. 4, we can see that $C'_{L_{rms}}$ results obtained numerically are not reliable but lie in the range between 0.1 and 0.7. Results obtained numerically can be considered reasonable, since we have $St \sim 0.19$, that $\overline{C_D} \sim 1.2$ and $0.3 < C'_{L_{rms}} < 0.4$.

Regarding the computational cost and feasibility EVM-RB-VMS-2 (Small-large) and EVM-RB-VMS-5 (DCDD-like) computational times are comparable to those of SUPG/PSPG/LSIC and RB-VMS and EVM-RB-VMS-3 (Large-large) computational time is considerably larger than those. EVM-RB-VMS-4 (Plateau) mean results are reasonable, but since convergence criteria were not achieved during the run, the resulting lift and drag curves are not presented. For EVM-RB-VMS-6 (One-one) we were not able to achieve convergence when using the same time step.

5 Conclusion and Future works

In this study we have presented a family of eddy viscosity models to be applied in a RB-VMS framework with two scales. Six different models were presented and tested. The classical example of the flow around a circular cylinder (with Reynolds number equals 1000) was used as test case. Time-averaged drag coefficient, time-averaged lift coefficient, root-mean-square lift force fluctuations and Strouhal number were presented for each of the resulting formulations as well as curves for lift and drag coefficients over time. The results were compared with those obtained with SUPG/PSPG/LISC with Smagorinsky eddy viscosity and those obtained with RB-VMS with no eddy viscosity. The presented formulations were implemented in EdgeCFD, an existing highly optimized code. We noted that four of the six implementations were able to represent turbulent flows with reasonable accuracy when compared with highly resolved numerical simulations and experimental data. We have also shown that these EVM-RB-VMS implementations have a computational performance comparable with the SUPG/PSPG/LSIC formulation with a classical Smagorinsky model and with the RB-VMS.

Further studies should consider mesh refinement tests, time step tests, other test cases, comparison for higher Reynolds numbers and analysis in the frequency domain in order to better evaluate the performance and accuracy of the presented formulations.

Acknowledgements

This research was supported by CNPq. Computer resources at Lobo Carneiro super computer were provided by the High-Performance Computer Center, COPPE/UFRJ

References

[1] Sagaut P, Deck S, Terracol M. Multiscale and Multiresolution Approaches in Turbulence. Imperial College Press: London, 2006.
[2] Lins EF, Elias RN, Guerra GM, Rochinha FA, Coutinho ALGA. Edge-Based Variational Multiscale Implementation of the Residual-Based Variational Multiscale Method. International Journal for Numerical Methods in Fluids 61(1):1-22. DOI:10.1002
[3] Pope SB. Turbulent Flows. Cambridge University Press: Cambridge 2000
[4] Hughes TJR, Feijóo GR, Mazzei L, Quincy J-B. The variational multiscale method - a paradigm for computational mechanics. Comput Methods Appl Mech Eng 166(1–2):3–24, 1998
[5] Hughes TJR, Calo VM, Scovazzi G. Variational and multiscale methods in turbulence. In: Mechanics of the 21st Century, pages 153–163. Springer, 2005
[6] Rasthofer U, Gravemeier V. Recent Developments in Variational Multiscale Methods for Large-Eddy Simulation of Turbulent Flow. Archives of Computational Methods in Engineering, 2017
[7] Elias RN, Coutinho ALGA, ALVES JLD, & AL. Recent Andvances In EdgeCFD on Wave-Structure Interaction and Turbulence Modeling. Marine Systems &Ocean Technology 9(1):49-58
[8] Oberai AA, Liu J, Sondak D, Hughes TJR. A residual based eddy viscosity model for the large, eddy simulation of turbulent flows, ICES REPORT 12-35, The Institute for Computational Engineering and Sciences, The University of Texas at Austin, 2012.
[9] Liu, J. Residual-based variational multiscale models for the large eddy simulation of compressible and incompressible turbulent flows, PhD. Thesis, Faculty of Rensselaer Polytechnic Institute, Troy, New York, 2012
[10] Oberai AA, Hughes TJR. A Palette of Fine-Scale Eddy Vscosity and Residual-Based Models for Variational Multiscale Formulation of Turbulence. Comput Mech 57:629-635
[11] Guerra GM, Rochinha FA, Coutinho ALG. Length-scale Smagorinsky models for LES-Stabilized finite element computation of turbulent flows, XXIX CILAMCE, 2008
[12] Elias RN, Coutinho ALGA. Stabilized Edge-Based Finite Element Simulation of Free-Surface Flows. International Journal for Numerical Methods in Fluids 54:965-993
[13] Smagorinsky J. General circulation experiments with primitive equations, part i: the basic experiment". Monthly Wea. Rev., 91, pp. 99-152, 1963
[14] Lilly DK. On the application of the eddy viscosity concept in the inertial subrange of turbulence. Technical report, NCAR manuscript 123, Boulder, 1966
[15] Silva RM, Lima B, Camata J, Lima, Elias RN, Coutinho ALGA. Communication-Free Parallel Mesh Multiplication for Large Scale Simulations", 13th International Meeting on High Performance Computing for Computational Science, VECPAR 2018, 2018
[16] Silva RM, Elias RN, Coutinho ALGA. Finite Element Mesh Multiplication with Boundary Smoothing, II Congresso Brasileiro de Fluidodinâmica Computacional, CBCFD 2018, 2018
[17] Gesenhues L, CamataJose J, Camata, Coutinho ALGA. Simulation of a column collapse for dense Ggranular flows, CILAMCE 2017 – XXXVIII, 2017
[18] Tezduyar TE. Computation of moving boundaries and interfaces and stabilization parameters. Int J Numer Methods Fluids 43(5):555–575, 2003
[19] Blevins RD. Flow Induced Vibration. Van Nostrand Reinhold Company New York, 1977
[20] Mittal S, Kumar V. Flow induced vibrations of a light circular cylinder at reynolds numbers 103 to 104. Journal of Sound and Vibration, 245, pp. 923–946, 2001
[21] Rosetti GF, Vaz G, Fujarra, ALC. URANS Calculations for Smooth Circular Cylinder Flow In A Wide Range Of Reynolds Numbers: Solution Verification And Validation, Journal of Fluids Engineering, Vol. 134, 121103, 2012
[22] Santos ML, Coutinho ALGA, Pfeil M. Vortex Shedding by LES 3D Numerical Simulation, CILAMCE 2017, 2017
[23] Massey BS, Mechanics of Fluids 4th ed Van Nostrand Reinhold, New York, 1979
[24] Klamo JT. Effects of Damping and Reynolds Number onVortex-Induced Vibrations, PhD. Thesis, California Institute of Technology, California, 2007
[25] Norberg C. Flow around a circular cylinder: aspects of fluctuating lift. Journal of Fluids and Structures 15, 459–469, 2001